Supporting information for:

Hetero-bimetallic Metal-organic Polyhedra

Jesse. M. Teo,[a] Campbell J. Coghlan,[a] Jack D. Evans,[a] Ehud Tsivion,[b] Martin Head-Gordon,[b] Christopher J. Sumby[a] and Christian J. Doonan[a]

[a.] *The Centre for Advanced Nanomaterials, School of Physical Sciences, University of Adelaide, Adelaide, Australia, 5005 Australia.*

[b.] *Department of Chemistry, University of California Berkeley, Berkeley, California 94720, United States.*

Table of Contents

Experimental Section

Materials and Measurements

Unless otherwise stated, all chemicals were obtained from commercial sources and used as received. DMA and MeOH were distilled from CaH_2 and degassed with Ar. Acetone was dried over $CaSO_4$ and distilled under Ar. Thermogravimetric analyses (TGA) were performed on a Perkin−Elmer STA-6000 instrument under a constant flow of N_2 at a temperature increase rate of 10 °C/min. Infrared spectra were recorded on a Perkin−Elmer Fourier-transform infrared (FT-IR) spectrometer on a zinc−selenide crystal. MOP samples for acid digestion analysis were dissolved in d^6-DMSO (1 mL) containing 1 drop of DCl solution (45% in D_2O). NMR spectra were recorded on a Varian 500 MHz spectrometer at 23 °C using a 5 mm probe. Powder X-ray diffraction data were collected on a Bruker Advanced D8 diffractometer (capillary stage) using Cu Kα radiation (λ = 1.5418 Å, 50 kW/40mA, 2θ = 2 – 55°). Energy-dispersive X-ray spectroscopy (EDX) was performed on a Philips XL30 field emission scanning electron microscope. Supercritical CO_2 activation was conducted using a Samdri-PVT-3D Critical-Point-Dryer.

Synthetic Methods

Precursor Hetero-bimetallic Acetate Synthesis

$[Pd(\mu\text{-}OAc)_4Cu(OH_2)(HOAc)_2]$, $[Pd(\mu\text{-}OAc)_4Ni(OH_2)(HOAc)_2]$ and $[Pd(\mu\text{-}OAc)_4Zn(OH_2)(HOAc)_2]$ were synthesised according to literature procedures.[1]

Cu_2(L) MOP

Cu_2(L) was prepared according to a literature procedure.[2]

NiPd(L) MOP

In a screw cap vial, $[Pd(\mu\text{-}OAc)_4Ni(OH_2)(HOAc)_2]$ (50 mg, 0.09 mmol) and 5-*tert*-butylisophthalic acid (20.6 mg, 0.09 mmol) were combined and sonicated in DMA (4 mL) for 2 min. The mixture was left at room temperature for 20 days resulting in orange prism-shaped crystals (35 mg, after activation). ν_{max}(neat, cm^{-1}): 2964(w), 1623(s), 1550(m), 1436(m), 1347(s), 1269(m) 911(w);

CuPd(L) MOP

In a screw cap vial, $[Pd(\mu\text{-}OAc)_4Cu(OH_2)(HOAc)_2]$ (50 mg, 0.09 mmol) and 5-*tert*-butylisophthalic acid (20.6 mg, 0.09 mmol) were combined and sonicated in DMA (4 mL) for 2 min. The mixture was left at room temperature for 2 days resulting in green prism-shaped crystals (18 mg after activation). ν_{max}(neat, cm^{-1}): 2960(w), 1610(s), 1550(m), 1414(m), 1356(s), 1265(m) 911(w);

ZnPd(L) MOP

In a screw cap vial, $[Pd(\mu\text{-}OAc)_4Zn(OH_2)(HOAc)_2]$ (50 mg, 0.09 mmol) and 5-*tert*-butylisophthalic acid (20.6 mg, 0.09 mmol)) were combined and sonicated in DMA (4 mL) for 2 min. The mixture was left at room temperature for 2 days resulting in pale yellow prism-shaped crystals (28 mg, after activation). ν_{max}(neat, cm^{-1}): 2962(w), 1605(m), 1586(m), 1401(m), 1349(s), 1268(m), 912(w);

Table 1. Metal content of bimetallic MOPs as measured by EDX analysis.

MOP	M (At %)	Pd (At%)
NiPd(L)	49.19	50.81
ZnPd(L)	48.30	51.70
CuPd(L)	61.52	38.48

Single Crystal X-ray Diffraction

Single crystals were mounted in paratone-N oil on a nylon loop. X-ray diffraction data were collected at 150(2) K with Mo Kα radiation (λ = 0.7107 Å) at 100(2) K on the MX-1 beamline of the Australian Synchrotron (λ = 0.7107 Å).[3] Data sets were corrected for absorption using a multi-scan method, and structures were solved by direct methods using SHELXS-2013, and refined by full-matrix least squares on F^2 by SHELXL-2014, interfaced through the program X-Seed.[4-7]

In general, all non-hydrogen atoms were refined anisotropically and hydrogen atoms were included as invariants at geometrically estimated positions, unless specified otherwise. While the hetero-bimetallic paddlewheels are incorporated into the MOPs with a significant preference for the palladium(II) centre on the interior surface, some disorder of these sites is observed by careful structural analysis. For each crystallographically unique paddlewheel the endohedral palladium and the exohedral 3d transition metal were refined at 75% occupancy and an endohedral 3d transition metal and exohedral palladium centre at 25% occupancy based on trial refinements. The minor paddlewheel component was refined using EXYZ and EADP restraints. The solvent molecule associated with each transition metal was assigned as an oxygen atom due to a high degree of disorder. DMA solvate molecules were disordered and refinement was accomplished using the SQUEEZE routine of Platon to remove electron density corresponding to these entities. Disorder of the *t*-butyl sites was also common to all the structures and was restrained accordingly.[8] All MOP crystals were only weakly diffracting despite the use of synchrotron radiation and this is noted as required for the individual structures.

Full details of the structure determinations have been deposited with the Cambridge Crystallographic Data Centre as CCDC #s 1423403-1423405. Copies of this information may be obtained free of charge from The Director, CCDC, 12 Union Street, Cambridge CB2 1EZ, U.K. (fax, +44-1223-336-033; e-mail, deposit@ccdc.cam.ac.uk).

Table 2. Crystal Data and Experimental X-ray Data for MPd(L) MOPs

Compound	CuPd(L)	NiPd(L)	ZnPd(L)
Empirical formula	$C_{288}H_{288}Cu_{12}O_{108}Pd_{12}$	$C_{288}H_{288}Ni_{12}O_{108}Pd_{12}$	$C_{288}H_{288}O_{108}Pd_{12}Zn_{12}$
Formula weight	7516.46	7458.49	7538.41
Crystal system	Tetragonal	Tetragonal	Tetragonal
Space group	*I*4/*m*	*I*4/*m*	*I*4/*m*
a (Å)	28.980 (4)	29.174 (4)	28.935 (4)
c (Å)	40.961 (8)	41.296 (8)	41.164 (8)
$\alpha = \beta = \gamma$ (°)	90	90	90
Volume (Å^3)	34400 (10)	35147 (12)	34464 (12)
Z	2	2	2
Density (calc.) (Mg/m^3)	0.726	0.705	0.726
Absorption coefficient (mm^{-1})	0.71	0.65	0.75
F(000)	7560	7536	7584
θ range for data collection (°)	1.0 to 22.7	1.0 to 24.7	1.0 to 20.7
Reflections collected	9612	12015	7333
Observed reflections	11778	15259	9079
[R(int)]	0.124	0.065	0.061
Restraints/parameters	9/495	8/494	9/494
Completeness (%)	0.998	0.937	0.998
Goodness-of-fit on F^2	1.04	1.07	1.04
R_1 [I>2σ(*I*)]	0.095	0.069	0.078
wR_2 (all data)	0.273	0.218	0.235
Largest diff. peak and hole (e.Å^{-3})	1.11	1.26	0.73

Table 3. Bond Lengths and angles for reported MOPs

Bond length (Å) or angle (°)	CuPd(L)	NiPd(L)	ZnPd(L)	CuCu(L)*
M-O(1)	1.986(8)	2.012(4)	2.027(6)	1.950(4)
M-O(5)	2.029(8)	2.016(4)	1.999(7)	1.962(4)
O1-M-O9	168.9(2)	170.93(13)	165.8(2)	168.56(19)
O5-M-O11	168.7(2)	171.17(13)	166.2(2)	168.56(19)
Pd1-O2	1.973(5)	2.004(3)	1.990(6)	1.942(4)
Pd1-O6	1.989(5)	1.990(3)	1.983(6)	1.954(4)
O2-Pd1-O10	174.4(2)	177.43(12)	176.9(2)	170.26(19)
O6-Pd1-O12	173.6(2)	177.28(12)	177.3(2)	170.26(19)
M-Pd/Cu(1)	2.5538(14)	2.4620(7)	2.5607(17)	2.594(17)
M-Pd/Cu(2)	2.5538(14)	2.4721(9)	2.5607(17)	2.663(2)

*Data retrieved from CCDC[2]

Powder X-ray Diffraction

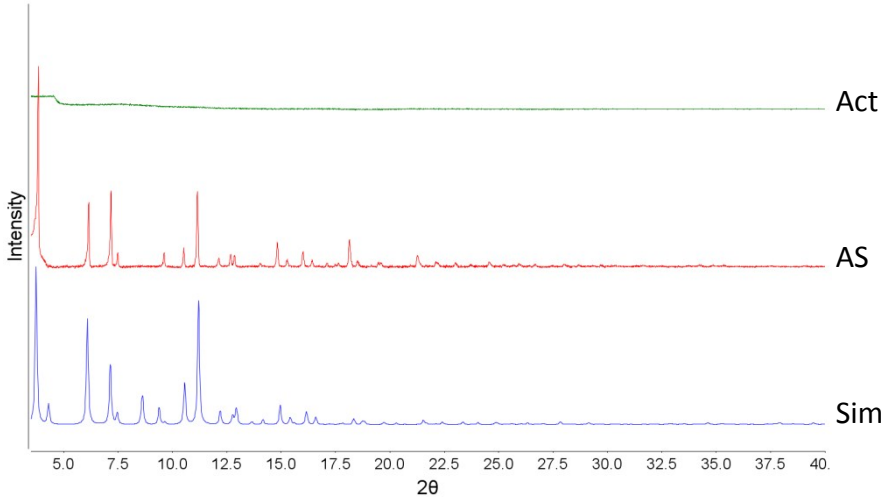

Figure 1. Powder X-ray diffraction of ZnPd(L) activated (green), as synthesised (red) and simulated from single crystal diffraction data (blue).

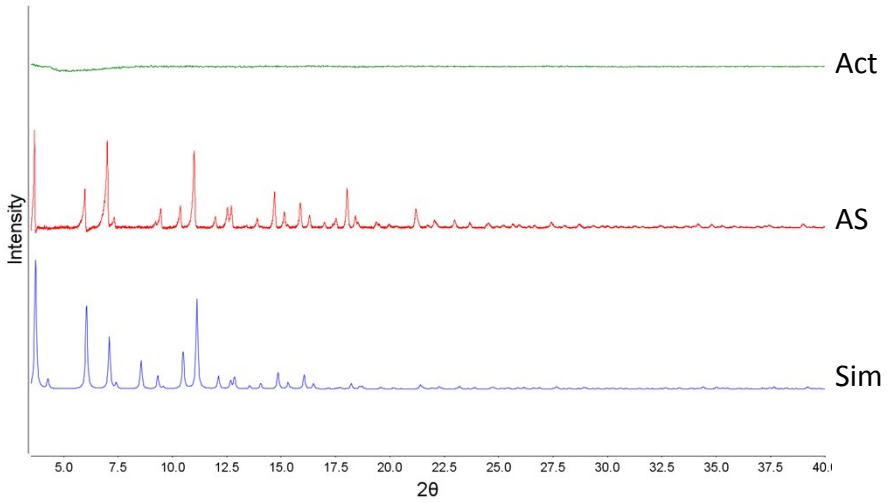

Figure 2. Powder X-ray diffraction of NiPd(L) activated (green), as synthesised (red) and simulated from single crystal diffraction data (blue).

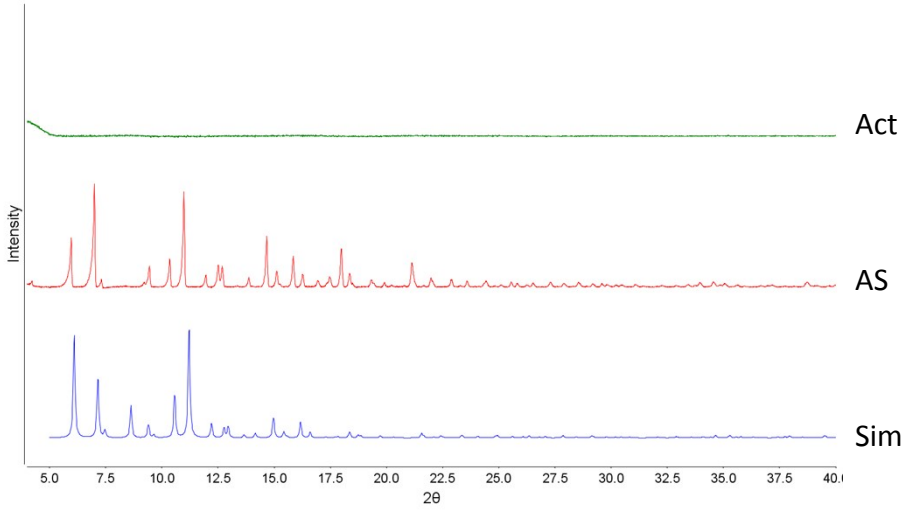

Figure 3. Powder X-ray diffraction of CuPd(L) activated (green), as synthesised (red) and simulated from single crystal diffraction data (blue).

Activation Protocol

Crystals of MPd(L) were washed in DMA (×3) over a 2 day period. The crystals were then exchanged into acetone (×7) over a 7 day period. The samples were dried with supercritical carbon dioxide and subsequently heated to 50°C for 200 min to yield the activated samples.

Thermogravimetric analysis, as described above, and NMR spectroscopy of digested, activated MOP samples were used to monitor activation.

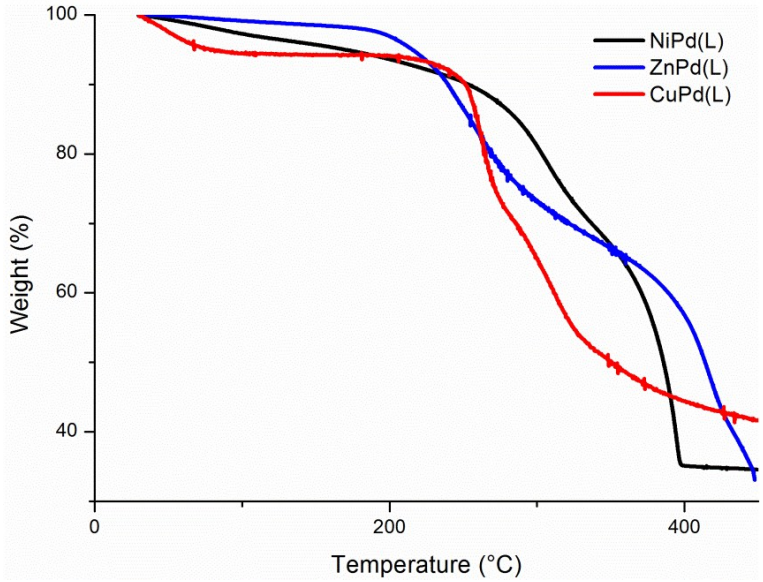

Figure 4. Thermogravimetric analysis of activated bimetallic MOPs.

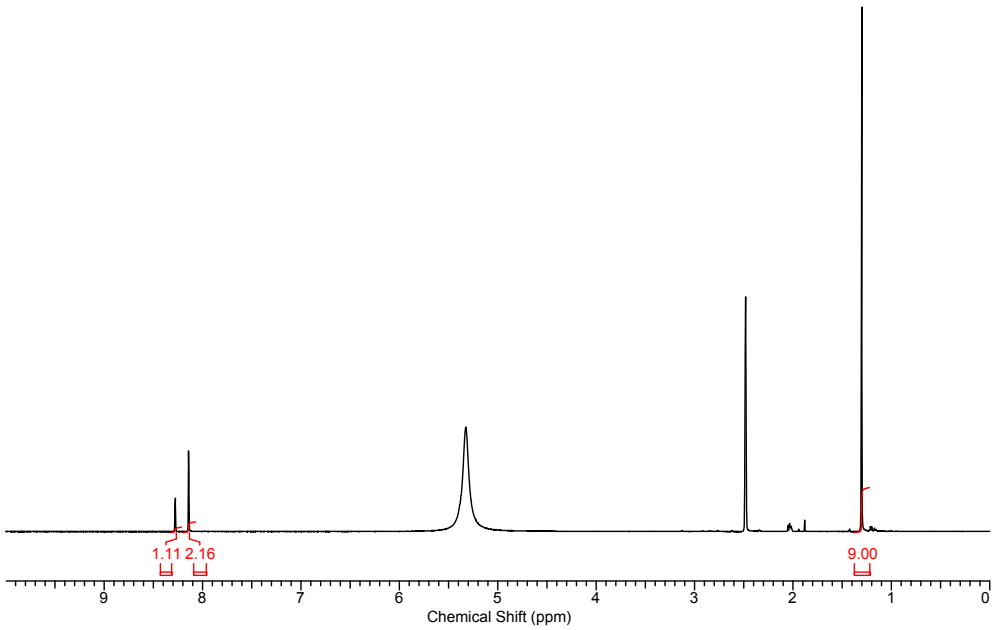

Figure 5. DCl *d*6-DMSO digested sample of activated ZnPd(L).

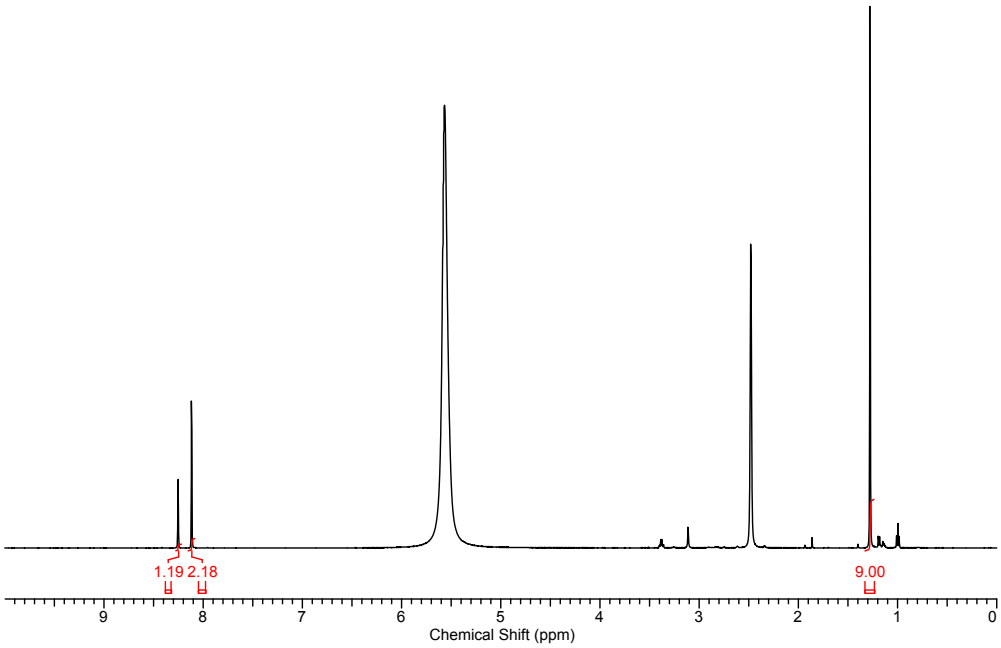

Figure 6. DCl *d*6-DMSO digested sample of activated NiPd(L).

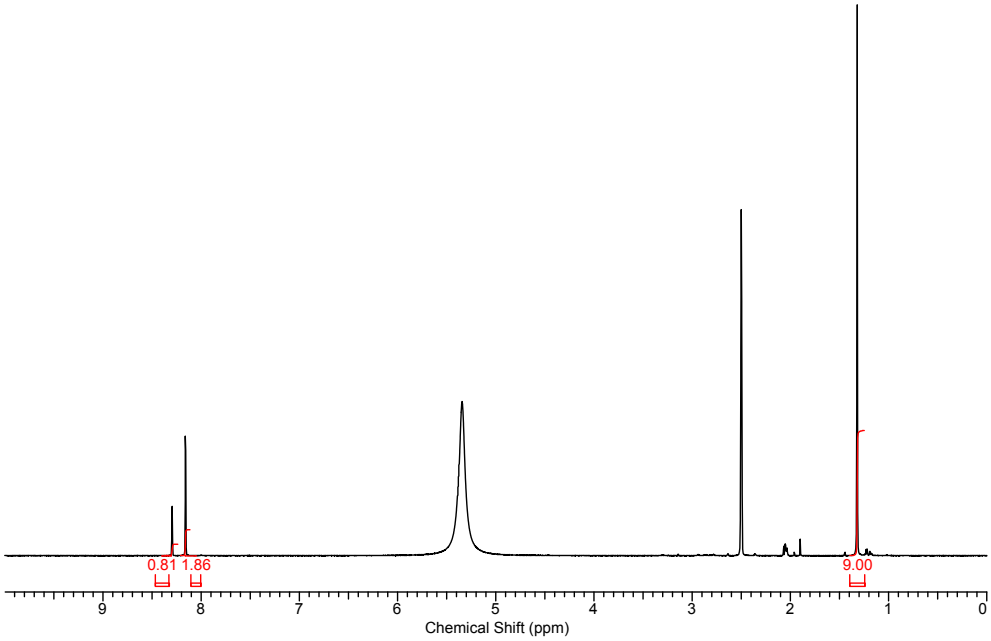

Figure 7. DCl *d*6-DMSO digested sample of activated CuPd(L).

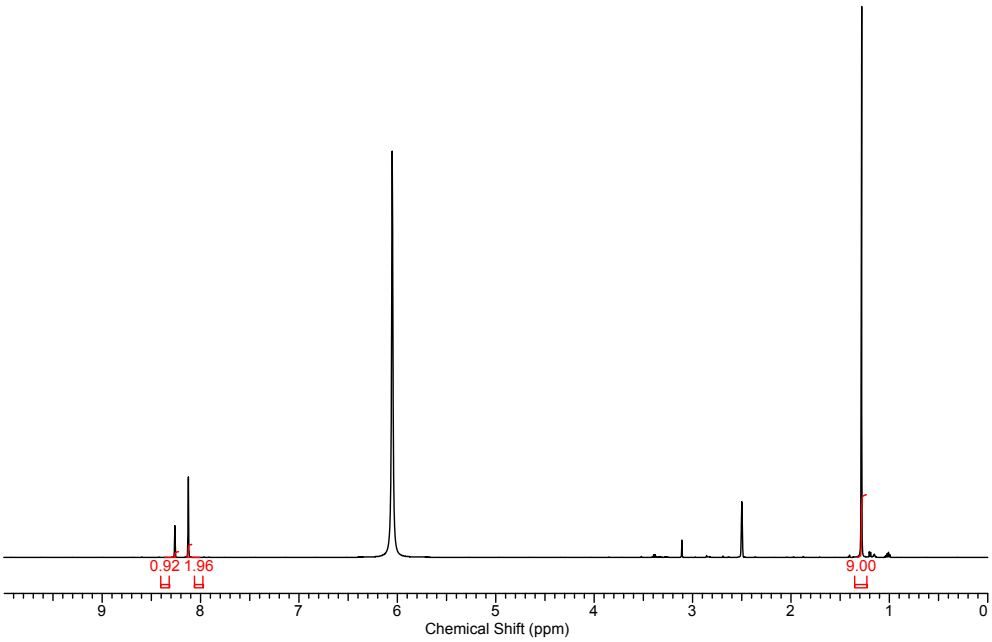

Figure 8. DCl *d*6-DMSO digested sample of activated Cu_2(L).

Gas Adsorption Measurements

Gas adsorption isotherms were measured using a Micromeritics 3-Flex or ASAP2020 analyzer (Micromeritics Instrument Corporation, Norcross, GA, USA) at 77 K and 87 K (utilizing liquid N_2 and Ar baths respectively or cryo-cooler circulator). Brunauer–Emmett–Teller (BET) surface areas and pore size distributions were calculated using software on the Micromeritics 3-Flex or ASAP2020 analyser. UHP grade (99.999%) N_2 and (99.999%) H_2 was used for all measurements.

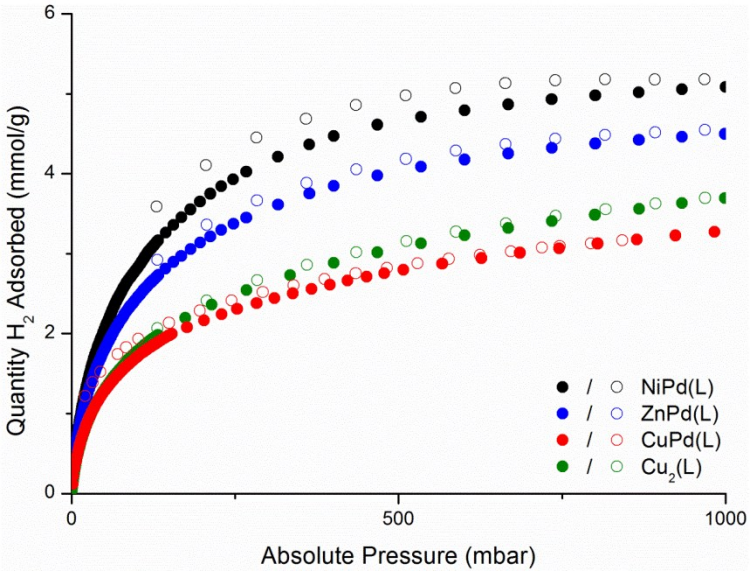

Figure 9. H_2 adsorption isotherms collected at 77 K for the bimetallic MPd(L) and Cu_2(L) MOPs following activation. Closed and open symbols represent adsorption and desorption data, respectively.

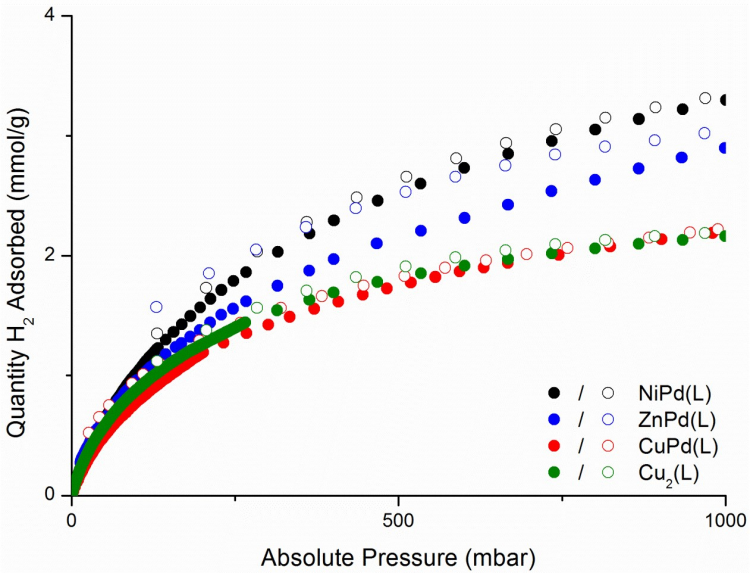

Figure 10. H_2 adsorption isotherms collected at 87 K for the bimetallic MPd(L) and Cu_2(L) MOPs following activation. Closed and open symbols represent adsorption and desorption data, respectively.

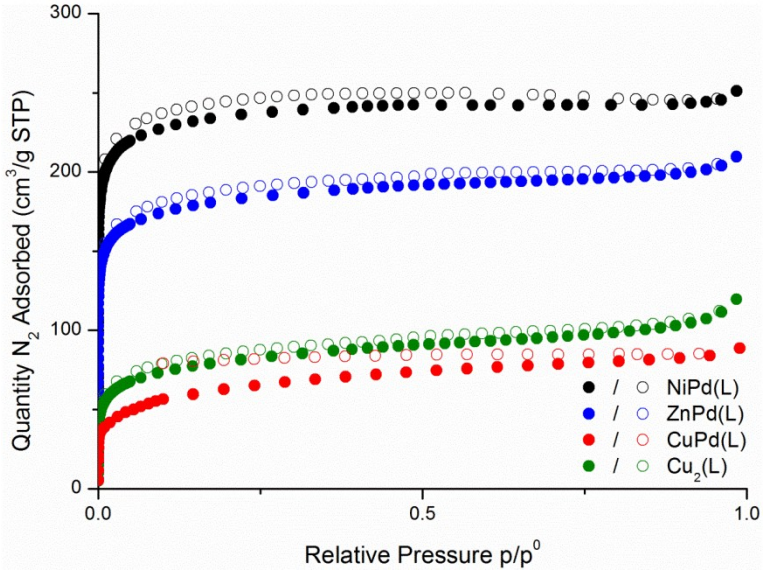

Figure 11. N_2 adsorption isotherms collected at 77 K for the bimetallic MPd(L) and Cu_2(L) MOPs following activation. Closed and open symbols represent adsorption and desorption data, respectively.

Structural Comparisons

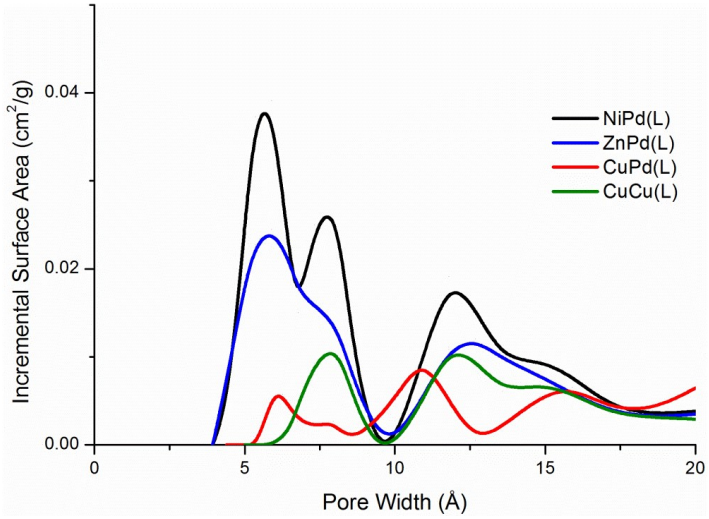

Figure 12. DFT pore size distributions determined from 77 K gas adsorption isotherms.

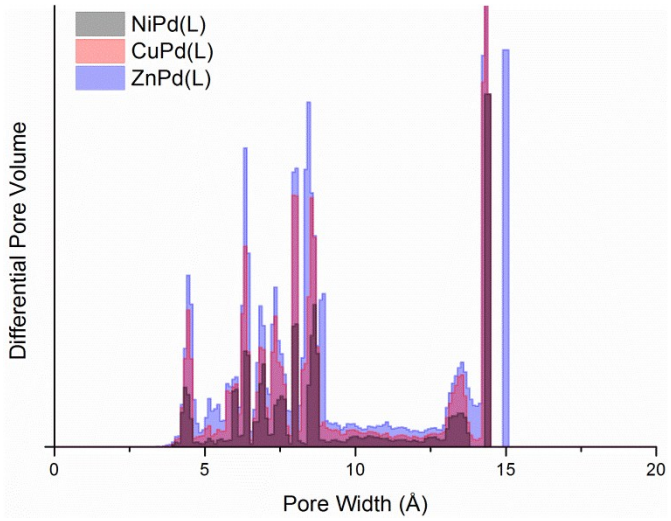

Figure 13. Simulated pore size distributions from the MOP single crystal structures.

Computational Data.

Computational Methods

Formate clusters were optimized with the B97-D functional[9] with empirical dispersion correction (D3)[10] and the def2-tzvpd[11, 12] basis set as employed by Gaussian09.[13] Very tight convergence criteria and ultrafine integration grid were used in all calculations. Additionally, benzoate and water solvated (at the Zn, Cu and Ni site) formate clusters (Figure 14) were optimized as to ensure there were no effects from the small formate cluster and the differences in geometry with respect to the crystal structure were a result of solvation. Optimized formate clusters using the B97-D3 functional were further compared to PBE0[14] and B3LYP*, which contains 15% exact exchange.[15] Notably, all functionals showed similar geometries to the crystal structure. Subsequently, the hydrogen interaction was investigated by optimizing formate clusters with a dihydrogen molecule placed above the transition metal to give a C2v symmetric dimer. The B97-D3/def2-tzvpd combination showed good agreement to the monomers and has been used to describe hydrogen adsorption in a number of analogous studies[16, 17] and thus used here. Hydrogen bound structures were optimized and verified to be a minimum on the potential energy surface with zero negative eigenvalue of the Hessian. Importantly, the Pd site showed no appreciable interaction with H_2 in many cases no minima was found. The bimetallic clusters were compared to the infamous CuCu cluster, which was modelled in the triplet state.[18] All hydrogen interaction energies were corrected for basis set superposition error[19] and zero-point energy contributions.

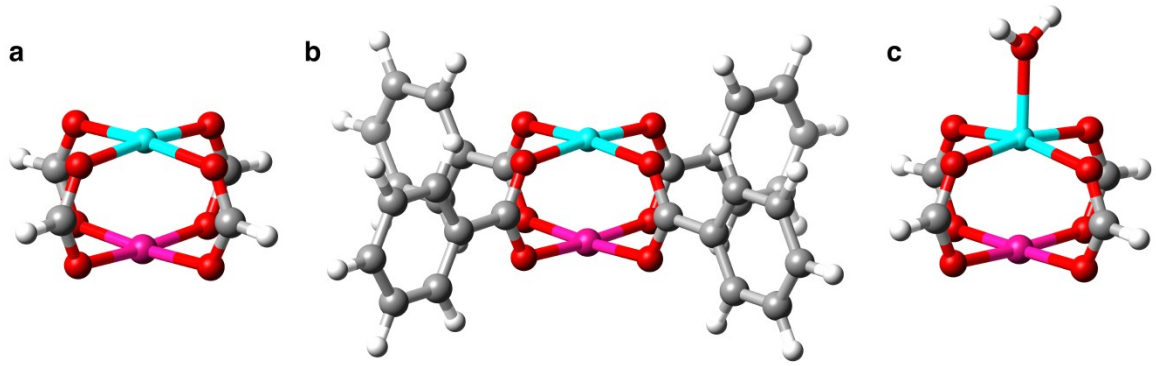

Figure 14. Clusters investigated by DFT methods: formate (a), benzoate (b) and water solvated (c).

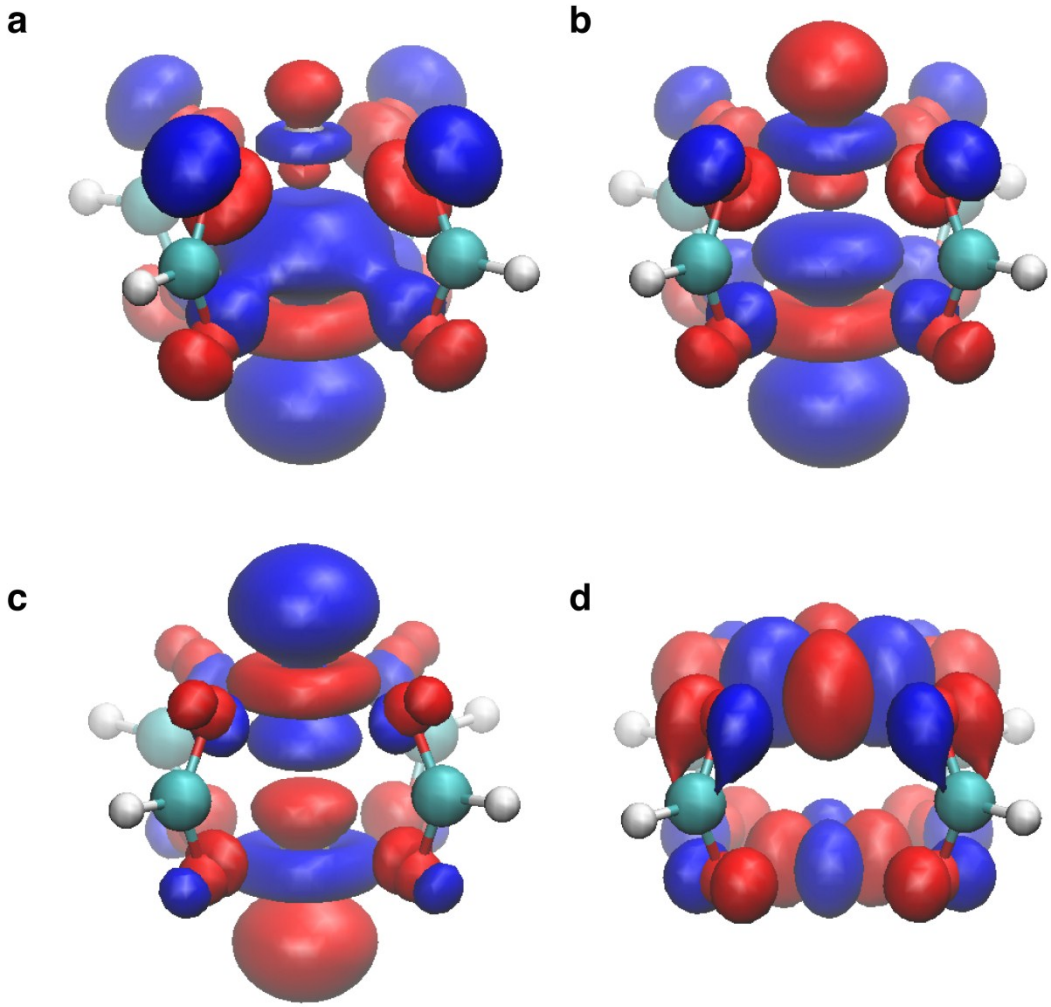

Figure 15. Highest occupied molecular orbitals for ZnPd, CuPd, NiPd(singlet) and NiPd(triplet) (a-d, respectively) generated at B97-D3/def2-tzvpd theory level.

Table 4. Calculated Parameters of Metal Formate Cluster at B97D3 level theory.

	Multiplicity	M-Pd / Å	O-M-O / °	O-Pd-O / °	Energy / Hartrees
ZnPd	Singlet	2.4805	173.8515	175.4116	-2665.16688
CuPd	Doublet	2.5139	173.5242	173.8338	-2526.17939
NiPd	Singlet	2.5151	176.2115	171.0287	-2393.90673
NiPd	Triplet	2.4188	175.0641	177.2961	-2393.91980

Table 5. Calculated Parameters of Metal Formate Cluster at PBE0 level theory.

	Multiplicity	M-Pd / Å	O-M-O / °	O-Pd-O / °	Energy / Hartrees
ZnPd	Singlet	2.4829	171.6798	175.6456	-2663.373156
CuPd	Doublet	2.3849	171.9434	180.6112	-2524.442078
NiPd	Singlet	2.4977	175.2427	171.0985	-2392.307431
NiPd	Triplet	2.4149	174.619	176.2754	-2392.332064

Table 6. Calculated Parameters of Metal Formate Cluster at B3LYP* level theory.

	Multiplicity	M-Pd / Å	O-M-O / °	O-Pd-O / °	Energy / Hartrees
ZnPd	Singlet	2.5194	172.7677	175.1249	-2656.079068
CuPd	Doublet	2.5465	173.1472	173.1507	-2517.383674
NiPd	Singlet	2.5481	175.5422	170.6049	-2385.402446
NiPd	Triplet	2.4535	174.8367	176.3603	-2385.417976

Table 7. Calculated Parameters of H_2O solvated Metal Formate Cluster at B97D3 level theory.

	Multiplicity	M-Pd / Å	O-M-O / °	O-Pd-O / °	Energy / Hartrees
ZnPd	Singlet	2.5474	166.7	178.9	-2741.619298
CuPd	Doublet	2.554	168.9	176.1	-2602.617503
NiPd	Singlet	2.491	176.3	171.6	-2470.334777
NiPd	Triplet	2.459	171.1	179	-2470.364396

Table 8. Calculated Parameters of Metal Benzoate Cluster at B97D3 level theory.

	Multiplicity	M-Pd / Å	O-M-O / °	O-Pd-O / °	Energy / Hartrees
ZnPd	Singlet	2.459	174	175.7	-3589.114209
CuPd	Doublet	2.49	173.7	174.2	-3450.128387
NiPd	Singlet	2.491	176.3	171.6	-3317.857261
NiPd	Triplet	2.397	175	177.9	-3317.869215

Hydrogen Interaction Energies and Binding Site Determination.

Table 9. Calculated Energies of Metal Formate – H_2 Interaction at B97D3 level theory.

	Multiplicity	H_2-M on M / Å	H-H on M / Å	Interaction Energy on M / kJ/mol
CuCu	Triplet	2.418	0.750	-6.54
ZnPd	Singlet	2.206	0.754	-8.81
CuPd	Doublet	2.434	0.750	-3.94
NiPd	Singlet	3.096	0.746	-2.04
NiPd	Triplet	1.998	0.760	-11.4

Table 10. Calculated Energies of Metal Formate – H_2 Interaction at PBE0 level theory.

	Multiplicity	H_2-M on M / Å	H-H on M / Å	Interaction Energy on M / kJ/mol
CuCu	Triplet	-2.293	0.752	-6.62
ZnPd	Singlet	-2.100	0.757	-9.69
CuPd	Doublet	-2.315	0.752	1.12
NiPd	Singlet	-2.933	0.747	0.795
NiPd	Triplet	-1.932	0.761	-13.8

Table 11. Hirshfeld Partial Charges at B97-D3 level theory.

	Muliplicity	M	O
CuCu	Triplet	0.424267	-0.239326
ZnPd	Singlet	0.453691	-0.25338
CuPd	Doublet	0.420878	-0.238996
NiPd	Singlet	0.204517	-0.202466
NiPd	Triplet	0.322829	-0.23347

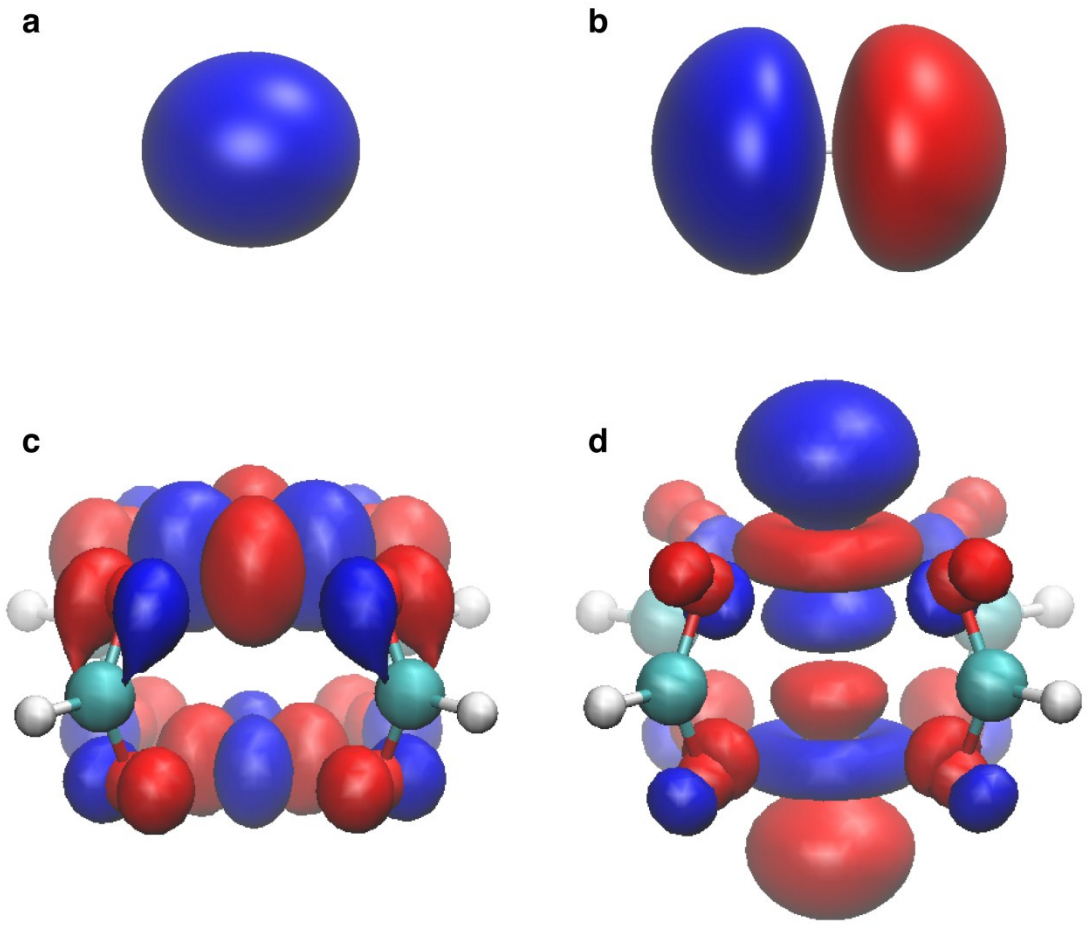

Figure 16. Orbitals that form a Kubas-type complex where there is donation from H_2 HOMO (a) to NiPd(triplet) LUMO (d) and back-donation from NiPd(triplet) HOMO (c) to the H_2 LUMO (b). Surfaces generated using B97-D3/def2-tzvpd theory.

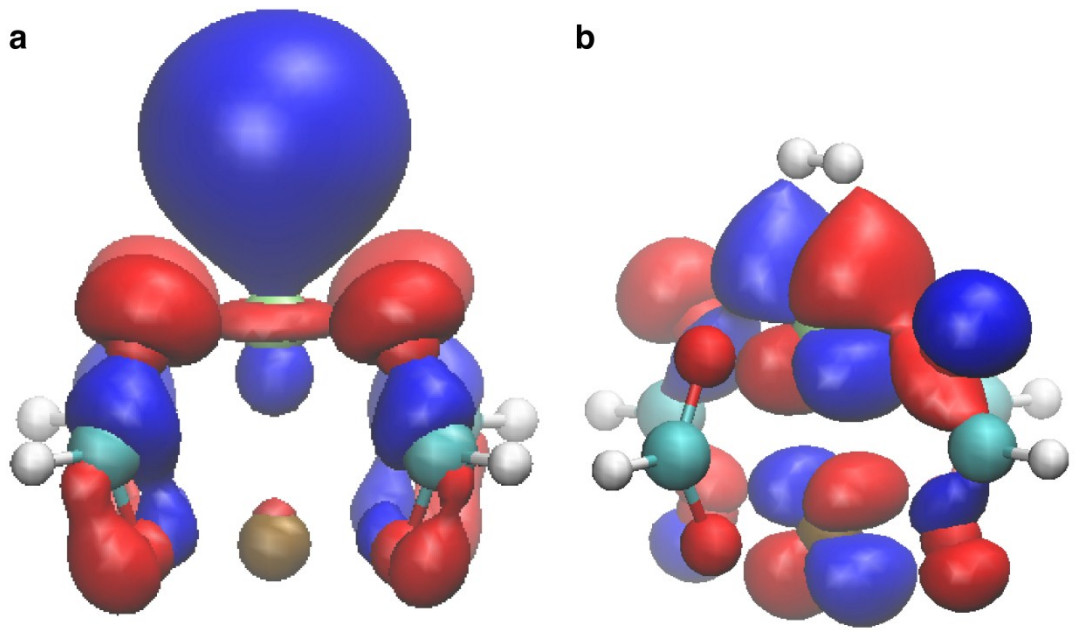

Figure 17. Occupied molecular orbitals of NiPd(triplet)-H_2 showing the Kubas bonding present in this interaction. Surfaces generated using B97-D3/def2-tzvpd theory.

References.

1. N. S. Akhmadullina, N. V. Cherkashina, N. Y. Kozitsyna, I. P. Stolarov, E. V. Perova, A. E. Gekhman, S. E. Nefedov, M. N. Vargaftik and I. I. Moiseev, *Inorg. Chim. Acta*, 2009, **362**, 1943-1951.
2. J.-R. Li and H.-C. Zhou, *Nat. Chem.*, 2010, **2**, 893-898.
3. T. M. McPhillips, McPhillips, S.E., Chiu, J. H., Cohen, A.E., Deacon, A. M., Ellis, P. J., Garman, E., Gonzalez, A., Sauter, N. K., Phizackerley, R. P., Soltis, S. M., Kuhn, P., *J. Synch. Rad.*, 2002, 401-406.
4. G. M. Sheldrick, University of Gottingen, 2014.
5. G. M. Sheldrick, *Acta Crystallogr.*, 2008, **A64**, 112.
6. G. M. Sheldrick, *Acta Crystallogr.*, 2015, **C71**, 3.
7. L. J. Barbour, *J. Supramol. Chem.*, 2001, **1**, 189-191.
8. A. L. Spek, *Acta Crystallogr.*, 2009, **D65**, 148-155.
9. S. Grimme, *J. Computational Chem.,* 2006, **27**, 1787-1799.
10. S. Grimme, J. Antony, S. Ehrlich and H. Krieg, *J. Chem. Phys.*, 2010, **132**, 154104.
11. D. Rappoport and F. Furche, *J. Chem. Phys.*, 2010, **133**, 134105.
12. F. Weigend and R. Ahlrichs, *Phys. Chem. Chem. Phys.*, 2005, **7**, 3297-3305.
13. M. Frisch, G. Trucks, H. Schlegel, G. Scuseria, M. Robb, J. Cheeseman, G. Scalmani, V. Barone, B. Mennucci and G. E. A. Petersson, *Gaussian 09 Revis. B01 Gaussian Inc Wallingford CT*, 2009.
14. C. Adamo and V. Barone, *J. Chem. Phys.*, 1999, **110**, 6158-6170.
15. J. Harvey, *Principles and Applications of Density Functional Theory in Inorganic Chemistry I*, Springer Berlin Heidelberg, 2004, **112**, 4, 151-184.
16. E. Tsivion, J. R. Long and M. Head-Gordon, *J. Am. Chem. Soc.*, 2014, **136**, 17827-17835.
17. L. Grajciar, P. Nachtigall, O. Bludský and M. Rubeš, *J. Chem. Theor. Comp.*, 2015, **11**, 230-238.
18. L. s. Grajciar, O. Bludský and P. Nachtigall, *J. Phys. Chem. Let.*, 2010, **1**, 3354-3359.
19. S. F. Boys and F. Bernardi, *Mol. Phys.*, 1970, **19**, 553-566.